The Journal of Infectious Diseases

MAJOR ARTICLE

Involvement of *Cryptosporidium parvum* Cdg7_FLc_1000 RNA in the Attenuation of Intestinal Epithelial Cell Migration via Trans-Suppression of Host Cell *SMPD3*

Zhenping Ming,[1,2] Ai-Yu Gong,[2] Yang Wang,[2] Xin-Tian Zhang,[2] Min Li,[2] Nicholas W. Mathy,[2] Juliane K. Strauss-Soukup,[3] and Xian-Ming Chen[2]

[1]Department of Medical Parasitology, School of Basic Medical Sciences, Wuhan University, Hubei, China; and [2]Department of Medical Microbiology and Immunology, School of Medicine, and [3]Department of Chemistry, College of Arts and Sciences, Creighton University, Omaha, Nebraska

Intestinal infection by *Cryptosporidium parvum* causes inhibition of epithelial turnover, but underlying mechanisms are unclear. Previous studies demonstrate that a panel of parasite RNA transcripts of low protein-coding potential are delivered into infected epithelial cells. Using in vitro and in vivo models of intestinal cryptosporidiosis, we report here that host delivery of parasite Cdg7_FLc_1000 RNA results in inhibition of epithelial cell migration through suppression of the gene encoding sphingomyelinase 3 (*SMPD3*). Delivery of Cdg7_FLc_1000 into infected cells promotes the histone methyltransferase G9a–mediated H3K9 methylation in the *SMPD3* locus. The DNA-binding transcriptional repressor, PR domain zinc finger protein 1, is required for the assembly of Cdg7_FLc_1000 into the G9a complex and associated with the enrichment of H3K9 methylation at the gene locus. Pathologically, nuclear transfer of *Cryptosporidium parvum* Cdg7_FLc_1000 RNA is involved in the attenuation of intestinal epithelial cell migration via trans-suppression of host cell *SMPD3*.

Keywords. *Cryptosporidium*; cryptosporidiosis; intestinal epithelium; parasitic infection; SMPD3; gene transcription; cell migration.

Cryptosporidium is an important opportunistic pathogen in patients with AIDS [1, 2]. While highly active antiretroviral therapy has reduced the incidence of cryptosporidiosis in developed countries with access to the treatment, it remains a significant AIDS-related opportunistic infection among people with a late diagnosis of human immunodeficiency virus infection or without access to the treatment [3, 4]. *Cryptosporidium* is also one of the most common pathogens (second to rotavirus) responsible for moderate-to-severe diarrhea in children aged <2 years in developing countries [5]. Infection shows significant association with mortality in this age group and appears to predispose children to lasting deficits in age-appropriate body growth and cognitive development [5, 6].

The primary infection site of *C. parvum* in human is the small intestine, one of the fastest regenerative tissues in the body [7]. The intestinal epithelium exhibits a remarkable capacity of self-renewal to maintain intestinal homeostasis; this property reflects the activity of intestinal stem cells in the crypt base [7]. New functional epithelial cells are produced from stem cells, differentiate, and migrate to the luminal surface, and hence, the entire intestinal epithelium is replaced every 2–3 days in mice (every 3–5 days in humans) [7]. Pathologically, one of the hallmarks of intestinal cryptosporidiosis is the inhibition of epithelial turnover and disturbances in cell metabolism [8, 9]. *C. parvum* infection triggers a mild inflammatory infiltration and causes a shorter height of the intestinal villi in the ileal epithelium [8].

Increasing evidence suggests that a certain portion of the eukaryotic genome is transcribed as non–protein-coding RNAs (ncRNAs) [10]. Some ncRNAs, such as microRNAs and the long ncRNAs, are functional and play key regulatory roles in diverse biological processes [11–13]. Many of these functional ncRNAs have been demonstrated to modulate gene expression at the transcriptional and posttranscriptional levels through recruitment of proteins or molecular complexes to specific loci, scaffolding of nuclear or cytoplasmic complexes, titration of RNA-binding proteins, or pairing with other RNAs [14, 15]. Recent genomic research has revealed the expression of novel ncRNA genes in the protozoan group of parasites. In eukaryotes, microRNAs induce posttranscriptional gene silencing via the RNA-interference pathway [11]. Members of the Apicomplexa protozoan parasites, such as *P. falciparum* and *C. parvum*, lack key components of the canonical Dicer-dependent RNA-interference pathway [16, 17]. Nevertheless, a panel of novel long ncRNAs has been identified in *P. falciparum* at the intraerythrocytic stage and select long ncRNAs have been demonstrated as emerging regulators in *P. falciparum* virulence gene expression [18, 19]. A detailed analysis of a full-length

Received 24 May 2017; editorial decision 31 July 2017; accepted 3 August 2017; published online August 7, 2017.

Correspondence: X.-M. Chen, MD, Department of Medical Microbiology and Immunology, Creighton University Medical Center, Criss III, Rm 352, 2500 California Plz, Omaha, NE 68178 (xianmingchen@creighton.edu).

The Journal of Infectious Diseases® 2018;217:122–33

DOI: 10.1093/infdis/jix392

complementary DNA library constructed from *C. parvum* identified 118 RNAs of low protein-coding potential [20, 21]. However, their functions in *C. parvum* biology and potential role in parasite-host interactions are unclear.

We recently made a novel observation that several *C. parvum* RNA transcripts of low protein-coding potential are selectively delivered into epithelial cells during host-parasite interactions and may modulate gene transcription in infected host cells [22]. One of these *C. parvum* RNA transcripts that are selectively delivered into the nuclei of infected host cells is the Cdg7_FLc_1000 transcript (GenBank accession number FX115830.1) [20, 21]. Sphingomyelin phosphodiesterase 3 (SMPD3), an enzyme encoded by *SMPD3* in humans, has been demonstrated to be associated with cell growth and migration [23, 24]. Here, we report that *C. parvum* infection attenuates intestinal epithelial cell migration with the involvement of parasite Cdg7_FLc_1000 RNA-mediated trans-suppression of host *SMPD3*.

METHODS

C. parvum and Cell Lines

C. parvum oocysts of the Iowa strain were purchased from a commercial source (Bunch Grass Farm, Deary, ID). INT cells (FHs 74 Int, CCL-241) and HCT-8 (CCL-244) were purchased from ATCC (Manassas, VA). HCT-8 cells stably expressing SMPD3 were obtained through transfection of cells with the pCMV6-Entry-SMPD3 (OriGene Technologies) and selection with G418, accordingly to the manufacturer's instruction. HCT-8 cells stably expressing the pCMV6-Entry vector were selected for control. Stable HCT-8-G9a$^{-/-}$ cells were generated and selected through transfection of cells with the G9a-CRISPR/Cas9 KO$^{(h)}$ and G9a-HDR plasmids (Santa Cruz).

Infection Models and Infection Assays

Cell-line models of intestinal cryptosporidiosis were used as previously described; infection was done with a 1:1 ratio of *C. parvum* oocysts to host cells [25]. A well-developed infection model of cryptosporidiosis in neonatal mice was used for in vivo experiments [26, 27]. At least 5 animals from each group were euthanized, and ileal tissues were obtained for immunohistochemical and biochemical analyses. Real-time polymerase chain reaction (PCR) analysis, immunofluorescence microscopy, and immunohistochemical analysis were used to assay *C. parvum* infection as previously reported [8, 25, 28]. Details are described in the Supplementary Materials.

Quantitative Real-Time PCR

For quantitative analysis of messenger RNA and *C. parvum* RNA expression, comparative real-time PCR analysis was performed as previous reported [28], using the SYBR Green PCR Master Mix (Applied Biosystems, Carlsbad, CA). Briefly, RNA was extracted using TRI-reagent, treated with a DNA-free kit (Ambion) to remove any remaining DNA. A total of 500 ng of quantified RNA was reverse transcribed using T100 thermal cyclers (Bio-Rad). Real-time PCR analysis was then performed using 25 ng of template complementary DNA for each RNA gene of interest. Each sample was run in triplicate. The relative abundance of each RNA was calculated using the $^{\Delta\Delta}$Ct method and normalized to *GAPDH* (total messenger RNA) or *U2* (nuclear RNA). The sequences for all primers are listed in Supplementary Table 1.

Small Interfering RNAs (siRNAs) and Plasmids

Custom-designed siRNA oligonucleotides against Cdg7_FLc_1000 and a scrambled siRNA were synthesized by Integrated DNA Technologies (Coralville, IA) and transfected into cells with lipofectamine RNAimax (Invitrogen). Sequences of siRNAs were 5'-GAGAUAACUAACGCCACCUUU-3' for Cdg7_FLc_1000 and nonspecific scrambled sequence UUCUCCGAACGUGUCACGUUU for the control. The Cdg7_FLc_1000 expression plasmid was generated by PCR amplification of Cdg7_FLc_1000 complementary DNA, using RNA from *C. parvum* sporozoites, and was cloned into the pcDNA3.1(+) vector, according to the manufacturer's protocol (Invitrogen). The sequences for all the primers are listed in Supplementary Table 1.

Whole-Cell, Cytoplasmic, and Nuclear Extract Preparation for Western Blot and Coimmunoprecipitation Analysis

Whole-cell extracts were prepared using the M-PER Mammalian Protein Extraction Reagent (Fisher) supplemented with cocktail protease inhibitors. Cell pellet was incubated in the M-PER Mammalian Protein Extraction Reagent and centrifuged at 16 100*g* for 20 minutes, and the supernatants were saved as the whole-cell extracts. Cytoplasmic and nuclear extracts were obtained using the standard approach [29]. Details are described in the Supplementary Materials.

RNA Immunoprecipitation, Chromatin Immunoprecipitation (ChIP), and Chromatin Isolation by RNA Purification

The formaldehyde–cross-linking RNA immunoprecipitation analysis was performed as described elsewhere [30]. For ChIP, a commercially available ChIP assay kit (Upstate Biotechnologies) was used in accordance with the manufacturer's instructions. Chromatin isolation by RNA purification analysis was performed as previously reported [14]. A pool of tiling oligonucleotide probes with affinity specific to the *C. parvum* Cdg7_FLc_1000 RNA sequences was used, and glutaraldehyde was cross-linked for chromatin isolation. The sequences for all the primers and probes are listed in Supplementary Table 1. Details are described in the Supplementary Materials.

Cell Migration and the MTT (3-[4,5-Dimethylthiazol-2-yl]-2,5-Diphenyltetrazolium Bromide) Assay

The wound-healing assay was used to analyze cell migration. A cell proliferation assay was performed using the CellTiter 96 Aqueous One Solution Cell Proliferation MTT assay kit (Promega), with details in the Supplementary Materials.

RESULTS

Nuclear Delivery of Parasite Cdg7_FLc_1000 RNA to Infected Epithelial Cells and Its Impact on Host Gene Transcription During *C. parvum* Infection

Cdg-FLc_1000 is from the parasite chromosome 7, with a sequence of 928 nucleotides from 2 exons (Supplementary Figure 1) [20, 21]. Using nonmalignant (INT) and malignant (HCT-8) human intestinal epithelial cells, we observed a similar infection burden between 2 cell lines 24, 36, and 48 hours after infection, as assessed by indirect immunofluorescence (Supplementary Figure 1). We also detected a significant amount of Cdg-FLc-1000 in the nuclear extracts from infected cells (Supplementary Figure 2). Overexpression of Cdg7_FLc-1000 in cells through transfection of Full-Cdg_FLc_1000 resulted in nuclear delivery (Supplementary Figure 2).

To explore the potential functional impact of Cdg7_FLc-1000 on host cells, we performed a genome-wide transcriptome analysis of INT cells after infection and after transfection of Full-Cdg7_FLc_1000. All array data were deposited in the GEO database (accession number GSE94128). Given that the impact of *C. parvum* infection on host cell gene transcription is generally very mild as compared to that of other pathogens [28, 31, 32], we chose fold changes of >1.25, combined with a *P* value of <.05 as the threshold, and identified 2068 genes that were upregulated in infected cells, compared with noninfected cells (Figure 1A and Supplementary Table 2). A total of 756 genes were significantly upregulated in cells after Full-Cdg7_FLc_1000 transfection, compared with cells transfected with the empty vector (Figure 1A and Supplementary Table 3). A total of 2292 and 653 genes were significantly downregulated in cells following infection and transfection with Full-Cdg7_FLc_1000, respectively (Figure 1A and Supplementary Tables 4 and 5). There were 180 overlapping upregulated genes and 119 overlapping downregulated genes in cells infected and transfected with Full-Cdg7_FLc_1000, respectively (Figure 1A and Supplementary Tables 6 and 7). Heat maps representing the top 50 overlapping genes that were either upregulated or downregulated are shown in Figure 1B). Expression levels of 3 upregulated genes (*CXCL2*, encoding C-X-C motif chemokine ligand; *IL6*, encoding interleukin 6; and *NFKBIZ*, encoding nuclear factor κ B inhibitor ζ) and 3 downregulated genes (*SMPD3,* the gene encoding lysyl oxidase-like 4 [*LOXL4*], and the gene encoding cadherin 3 [*CDH3*]) were further validated using real-time PCR in cells following infection or transfection with Full-Cdg7_FLc_1000 (Figure 1C). Of note, the expression levels of many genes were also altered in cells transfected with the empty vector, compared with the uninfected and untransfected control, presumably due to the transfection process.

Suppression of SMPD3 Expression in Host Cells Induced by *C. parvum* Infection Is Mediated by Delivery of Cdg7_FLc_1000

SMPD3 has been demonstrated to be associated with epithelial cell growth and migration [23, 24]. Therefore, we selected this gene to further explore its potential pathological significance in cryptosporidiosis. Downregulation of *SMPD3* was further confirmed using real-time PCR in cells following infection or transfection of Full-Cdg7_FLc_1000 for various periods (Figure 2A). Downregulation of SMPD3 at the protein level was detected in infected HCT-8 cells (Figure 2B). We then questioned whether nuclear delivery of Cdg7_FLc_1000 causes SMPD3 trans-suppression. Because *C. parvum* genes are very difficult, if not impossible, to modify with conventional genetic tools [1, 33], we developed an approach to treat cells with a siRNA to Cdg7_FLc_1000 for 12 hours and then exposed them to *C. parvum*. The increase of Cdg7_FLc_1000 RNA levels both in INT and HCT-8 cells induced by *C. parvum* infection was significantly suppressed by pretreatment of the siRNA to Cdg7_FLc_1000 (Figure 2C). Accordingly, suppression of SMPD3 RNA expression induced by *C. parvum* infection was at least partially attenuated through pretreatment of the siRNA to Cdg7_FLc_1000 (Figure 2D).

Nuclear Delivery of Cdg7_FLc_1000 Promotes G9a-Mediated H3K9 Methylation in the *SMPD3* Locus

Histone modifications, such as methylation by H3K9 and H3K27, are generally associated with gene transcriptional suppression [34]. Increased enrichment of H3K9me3 but not H3K27me3 was detected in the *SMPD3* locus in infected cells by using ChIP analysis with anti-H3K9me3 or anti-H3K27me3 and the PCR primer sets as designed to cover the various promoter regions of the *SMPD3* locus (Figure 3A). Similarly, increased enrichment of H3K9me3 but not H3K27me3 was detected in the *SMPD3* locus in cells after transfection of Full-Cdg7_FLc_1000 (Figure 3B). Furthermore, as assessed by Western blot, the level of H3K9me3 but not H3K27me3 was increased in cells following infection (Figure 3C). In a well-documented model of intestinal cryptosporidiosis, in which *C. parvum* was administered orally to neonatal mice [26, 27], increased staining of H3K9me3 was detected by immunohistochemical staining of infected intestinal tissues (Figure 3D).

The euchromatic histone lysine methyltransferase 2 (G9a), a histone methyltransferase for H3K9 methylation, mediates gene trans-suppression in many cell types [33]. We then questioned whether the recruitment of G9a protein within the *SMPD3* locus is related with its enrichment of H3K9me3. Increased recruitment of G9a to the *SMPD3* locus was detected in infected HCT-8 cells or cells transfected with Full-Cdg7_FLc_1000, using anti-G9a and the PCR primer sets as designed for ChIP analysis (Figure 4A). To define whether the enrichment of H3K9me3 depends on G9a, we generated a stable G9a$^{-/-}$ HCT-8 cell line, using the G9a-CRISPR/Cas9 KO$^{(h)}$ and G9a-HDR plasmids (Santa Cruz). Deletion of G9a in the stable G9a$^{-/-}$ HCT-8 cell line was confirmed by Western blotting (Figure 4B). Downregulation of *SMPD3* induced by *C. parvum* infection was not detected in the G9a$^{-/-}$ HCT-8 cells following infection (Figure 4C). Complementarily, knockdown of G9a attenuated the enrichment of H3K9me3 within the *SMPD3* locus in infected cells (Figure 4D).

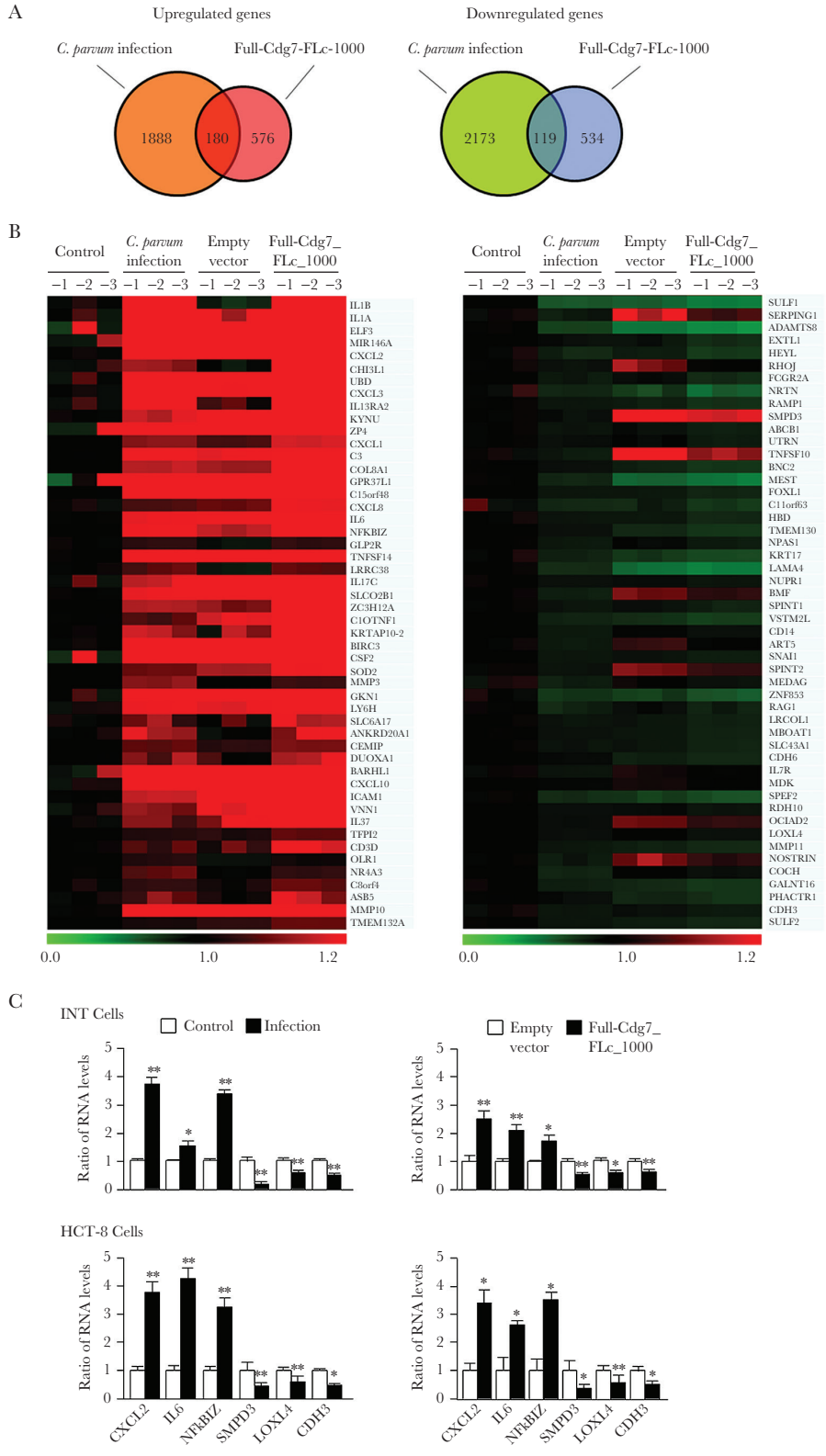

Figure 1. Alterations in host gene expression profiles in cells following *Cryptosporidium parvum* infection and overexpressing Cdg7_FLc_1000. *A*, Genome-wide transcriptome analysis in INT cells following *C. parvum* infection and transfection of Full-Cdg7_FLc_1000 for 48 hours, taking a fold change of >1.25 and a *P* value of <.05 as the threshold. The total numbers of genes whose expression is significantly altered after infection or transfection are shown. *B*, Heat maps representing the top 50 overlapping genes either upregulated or downregulated in cells following Full-Cdg7_FLc_1000 transfection and *C. parvum* infection. Expression Levels of RNAs are presented as fold changes to the mean value of the $\log_2$ (Hy5/Hy3) ratios in noninfected control. *C*, Altered expression levels of select genes in INT and HCT-8 cells were further validated by real-time polymerase chain reaction analysis. Data represent 3 independent experiments. **P*<.05 and ** *P*<.01, by analysis of variance, compared with noninfected or empty vector controls.

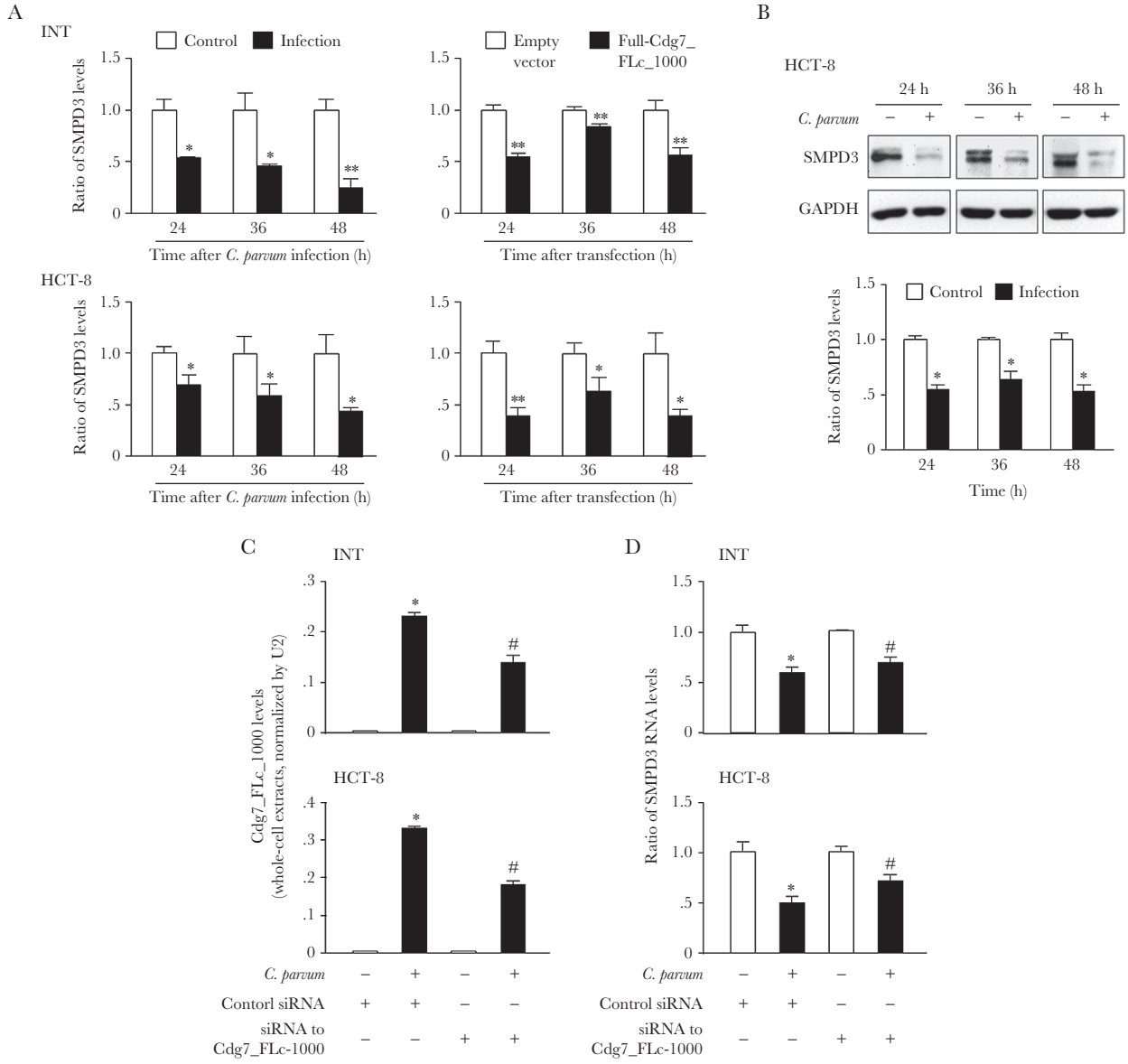

Figure 2. Downregulation of *SMPD3* in epithelial cells following *Cryptosporidium parvum* infection is associated with delivery of Cdg7_FLc_1000 into the infected host cells. *A,* Downregulation of *SMPD3* was further analyzed by real-time polymerase chain reaction (PCR) analysis in INT and HCT-8 cells following *C. parvum* infection or transfection of Full-Cdg7_FLc_1000 for various periods. **P*<.05, by *t*-test, compared with control; ***P*<.01, by *t*-test, compared with control. *B,* Content of SMPD3 in HCT-8 cells following *C. parvum* infection for 24, 36, and 48 hours, as assessed by Western blot. Representative gel images are shown, and densitometric levels of SMPD3 signal were quantified. GAPDH was blotted for control. **P*<.05, by *t*-test, compared with control. *C,* Inhibition of delivery of Cdg7_FLc_1000 into infected cells through pretreatment of host cells with a small interfering RNA (siRNA) to Cdg7_FLc_1000, followed by exposure of cells to *C. parvum* infection. INT and HCT-8 cells were treated with a siRNA to Cdg7_FLc_1000 for 12 hours and then exposed to *C. parvum* infection for additional 24 hours. Contents of Cdg7_FLc_1000 in the infected cells were quantified by quantitative real-time PCR analysis. A nonspecific scrambled siRNA was used as the control. *D,* Inhibition of Cdg7_FLc_1000 in host cells by the siRNA treatment attenuated the downregulation of *SMPD3* following *C. parvum* infection. INT and HCT-8 cells were treated with a siRNA to Cdg7_FLc_1000 for 12 hours and then exposed to *C. parvum* infection for additional 24 hours. Expression levels of SMPD3 in the infected cells were quantified by real-time PCR. Data represent 3 independent experiments. **P*<.01, by analysis of variance (ANOVA), compared with noninfected cells treated with the control siRNA; #*P*<.01, by ANOVA, compared with infected cells treated with the control siRNA.

PR Domain Zinc Finger Protein 1 (PRDM1) Is Involved in the Assembly of Cdg7_FLc_1000 Into the G9a Complex and Associated With the Enrichment of H3K9 Methylation at the *SMPD3* Gene Locus

We questioned whether the RNA-binding elements in the G9a complex may mediate the recruitment of Cdg7_FLc_1000 to the *SMPD3* locus. PRDM1 (also known as BLIMP-1) is a G9a-interacting protein [35] and an RNA-binding protein [36] that has been implicated in G9a-mediated histone methylation [37]. HCT-8 cells were exposed to *C. parvum* infection for 24 hours, followed by coimmunoprecipitation analysis. An increased physical association between G9a and PRDM1 was detected in infected cells (Figure 5A). To test whether Cdg7_FLc_1000 is assembled into the G9a/PRDM1 complex in the infected cells, we performed RNA immunoprecipitation analysis of infected

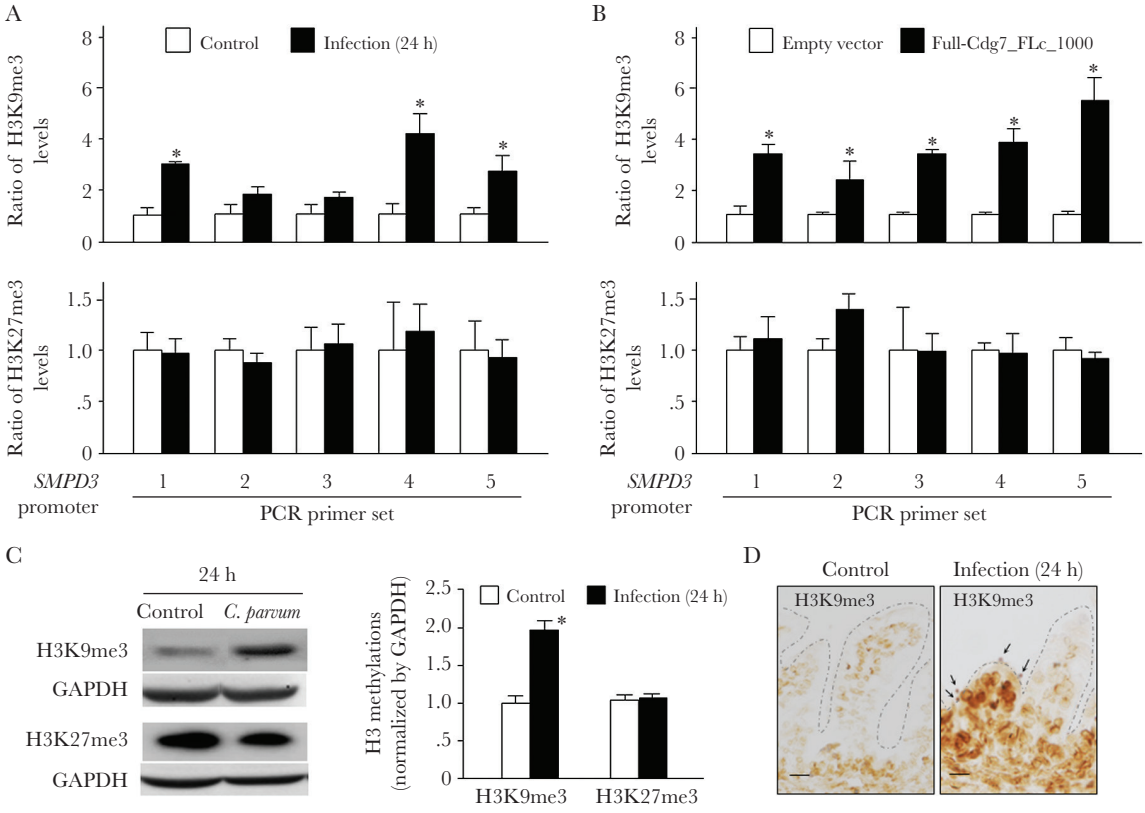

Figure 3. Enrichment of H3K9me3 within the *SMPD3* locus in cells following *Cryptosporidium parvum* infection or transfection of Full-Cdg7_FLc_1000. *A,* Levels of the suppression markers H3K9me3 and H3K27me3 associated with the *SMPD3* locus in HCT-8 cells following *C. parvum* infection. Cells were exposed to *C. parvum* infection for 24 hours, followed by chromatin immunoprecipitation (ChIP) analysis using anti-H3K9me3 or anti-H3K27me3 and the polymerase chain reaction primer sets as designed. Increased enrichment of H3K9me3 but not H3K27me3 was detected in the *SMPD3* locus in cells following infection. *B,* Levels of the suppressive markers H3K9me3 and H3K27me3 associated with the *SMPD3* locus in HCT-8 cells following transfection of Full-Cdg7_FLc_1000. Cells were transfected with Full-Cdg7_FLc_1000 for 24 hours, followed by ChIP analysis. The empty vector was used as the control. Similarly, increased enrichment of H3K9me3 but not H3K27me3 was detected in the *SMPD3* locus in the transfected cells. *C,* Levels of the suppressive markers H3K9me3 and H3K27me3 in HCT-8 cells following *C. parvum* infection, as assessed by Western blot. Cells were exposed to *C. parvum* infection for 24 hours, followed by Western blot for detection of H3K9me3 and H3K27me3. Representative gel images are shown, and densitometric levels were quantified. *D,* Increased H3K9me3 level in intestinal tissues in mice following *C. parvum* infection in vivo. Neonatal mice aged 6 days received *C. parvum* oocysts by oral gavage, and ileal tissues were obtained 24 hours after parasite administration. Immunohistochemical analysis yielded increased staining of H3K9me3 in the ileum from infected animals (parasites are indicated by arrows), compared with the noninfected control. Data represent means ± SEs from 3 independent experiments. The bar denotes 20 μm. **P*<.01, by analysis of variance, compared with noninfected or empty vector controls.

cells. A significant amount of Cdg7_FLc_1000 was detected in the immunoprecipitates from infected cells, using either anti-G9a or anti-PRDM1 (Figure 5B). Moreover, recruitment of PRDM1 to the *SMPD3* locus was detected in infected cells and cells transfected with Full-Cdg7_FLc_1000 (Figure 5C). To test whether Cdg7_FLc_1000 is physically recruited to the *SPMD3* locus in infected cells, we used a pool of biotinylated tiling oligonucleotide probes specific to Cdg7_FLc_1000 for chromatin isolation by RNA purification. Recruitment of Cdg7_FLc_1000 was detected within the *SMPD3* locus in cells following infection or transfection with Full-Cdg7_FLc_1000 (Figure 5D).

Attenuation of Intestinal Epithelial Cell Migration Following *C. parvum* Infection Involves Expression of *SMPD3*

Compared with noninfected controls, cell migration distance decreased significantly in *C. parvum*–infected cells (Figure 6A). Interestingly, cells along the migrating edge included both directly infected cells and noninfected cells, suggesting that inhibition of migration is not limited to infected cells only (Figure 6A). This decrease in the cell migration distance is not due to cell death induced by infection, as reported in previous studies [38, 39]. First, no obvious apoptosis was revealed by DAPI (4′,6-diamidino-2-phenylindole) staining in the infected cell cultures (Figure 6A). Second, the MTT assay revealed no obvious difference between the infected cell cultures and the noninfected controls (Figure 6A). The lack of obvious cell death may reflect the higher infection rate and the fully confluent nature of the cells, as *C. parvum*–infected cells and cells under confluent conditions are resistant to apoptosis [39]. We then established a HCT-8 cell line stably expressing SMPD3, as confirmed by PCR and Western blot (Figure 6B). HCT-8 cells stably expressing the empty vector (pCMV6-Entry) were used as the control. Of note, the transfection process by itself decreased the

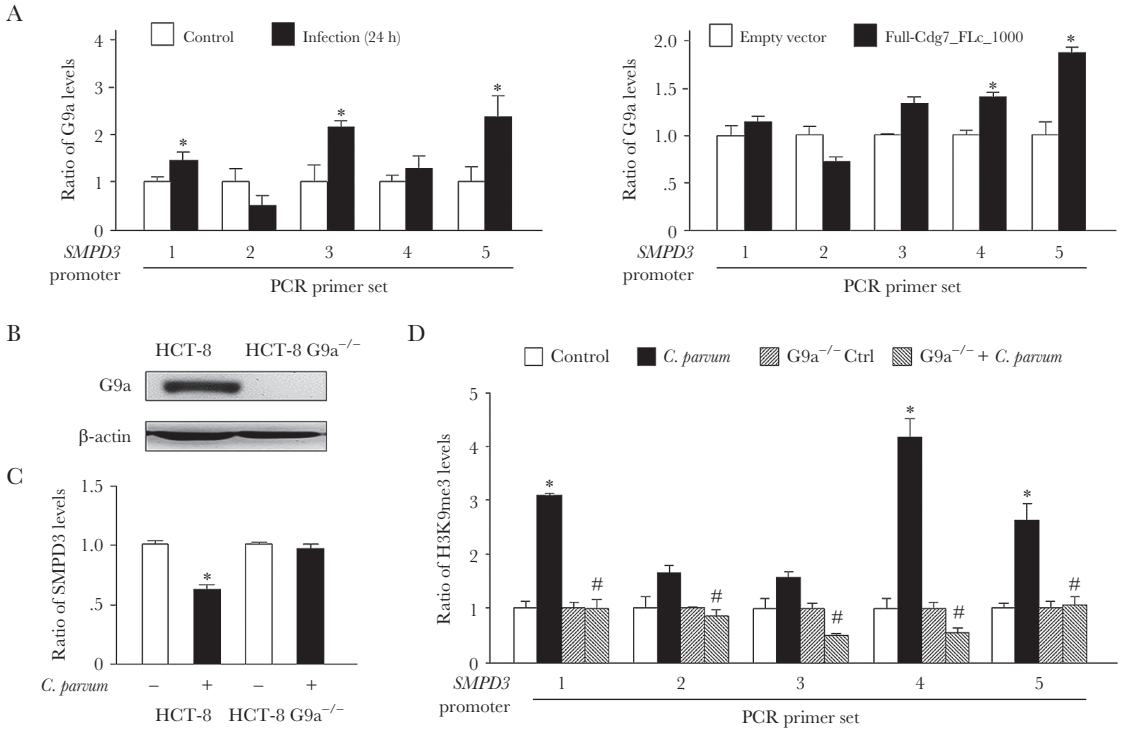

Figure 4. Enrichment of H3K9me3 within the *SMPD3* locus in cells following *Cryptosporidium parvum* infection involves the recruitment of G9a. *A,* Increased recruitment of G9a to the *SMPD3* locus in HCT-8 cells following *C. parvum* infection or transfection with Full-Cdg7_FLc_1000. Cells were exposed to *C. parvum* infection for 24 hours or transfected with Full-Cdg7_FLc_1000 for 24 hours, followed by chromatin immunoprecipitation (ChIP) analysis using anti-G9a and the polymerase chain reaction (PCR) primer sets as designed. Increased recruitment of Ga9 was detected in the *SMPD3* locus in cells following infection or Full-Cdg7_FLc_1000 transfection. *B,* Knockdown of *G9a* in HCT-8 cells. Cells were transfected with the G9a-CRISPR/Cas9 KO$^{(h)}$ and G9a-HDR plasmids; stably transfected cells were cloned and confirmed by Western blot analysis. *C,* Knockdown of *G9a* attenuated the downregulation of *SMPD3* in cells following *C. parvum* infection. The SMPD3 RNA levels were quantified in HCT-8 and HCT-8-G9a$^{-/-}$ cells after exposure to *C. parvum* infection for 24 hours, using real-time PCR analysis. *D,* Knockdown of *G9a* attenuated the enrichment of H3K9me3 within the *SMPD3* locus in cells following *C. parvum* infection. HCT-8 and HCT-8-G9a$^{-/-}$ cells were exposed to *C. parvum* infection for 24 hours. Levels of H3K9me3 associated with the *SMPD3* locus were assessed by ChIP analysis. Data represent means ± SEs from 3 independent experiments. **P*<.05, by analysis of variance (ANOVA), compared with noninfected controls or empty vector controls; #*P*<.05, by ANOVA, compared with infected controls.

distance of cell migration (Supplementary Figure 3). Whereas a higher migration distance was detected in cells stably expressing SMPD3 (Figure 6C), a similar migration dynamic was observed for cells stably expressing SMPD3 following infection, compared with the noninfected cells (Figure 6C and 6D), suggesting that overexpression of SMPD3 attenuated the inhibition of cell migration induced by infection. No difference in cell proliferation was detected in cells among all the treated groups (Figure 6C). Finally, we detected a significant decrease in the ileal villus heights, accompanied with an expansion of the crypt region, in the ileal epithelium of neonatal mice after oral administration of *C. parvum* oocysts (Figure 7A and 7B). We observed decreased staining of Smpd3 in epithelial cells covering the villi of the infected ileal epithelium, whereas the noninfected crypts and the submucosal regions showed a similar higher level of Smpd3 staining, comparable to staining in corresponding noninfected intestinal tissues (Figure 7C). Accordingly, decreased expression levels of Smpd3 RNA were detected in infected ileal tissues (Figure 7D).

DISCUSSION

The interactions between *Cryptosporidium* and intestinal epithelial cells may involve exchanges of distinct effector molecules from either side at the host-parasite interface. *C. parvum* discharge of rhoptry and microneme contents, a conserved strategy of host cell entry for all Apicomplexa, occurs at the initial stage of infection, which presumably facilitates parasite entry and parasitophorous vacuole formation [40]. Several parasite proteins have been demonstrated to be delivered into host epithelial cells at the host-parasite interface and are involved in parasite intracellular development [40, 41]. Recent observation of delivery of *C. parvum* RNA transcripts of low protein-coding potential into infected host cells expands the exchanged effector molecule list to include specific parasite RNAs at the *C. parvum*–host cell interfaces [23]. Our data support the notion that cryptosporidial infection induces epigenetic histone methylations in infected cells through nuclear transfer of specific parasite RNAs, resulting in transcriptional suppression of genes with pathological significance.

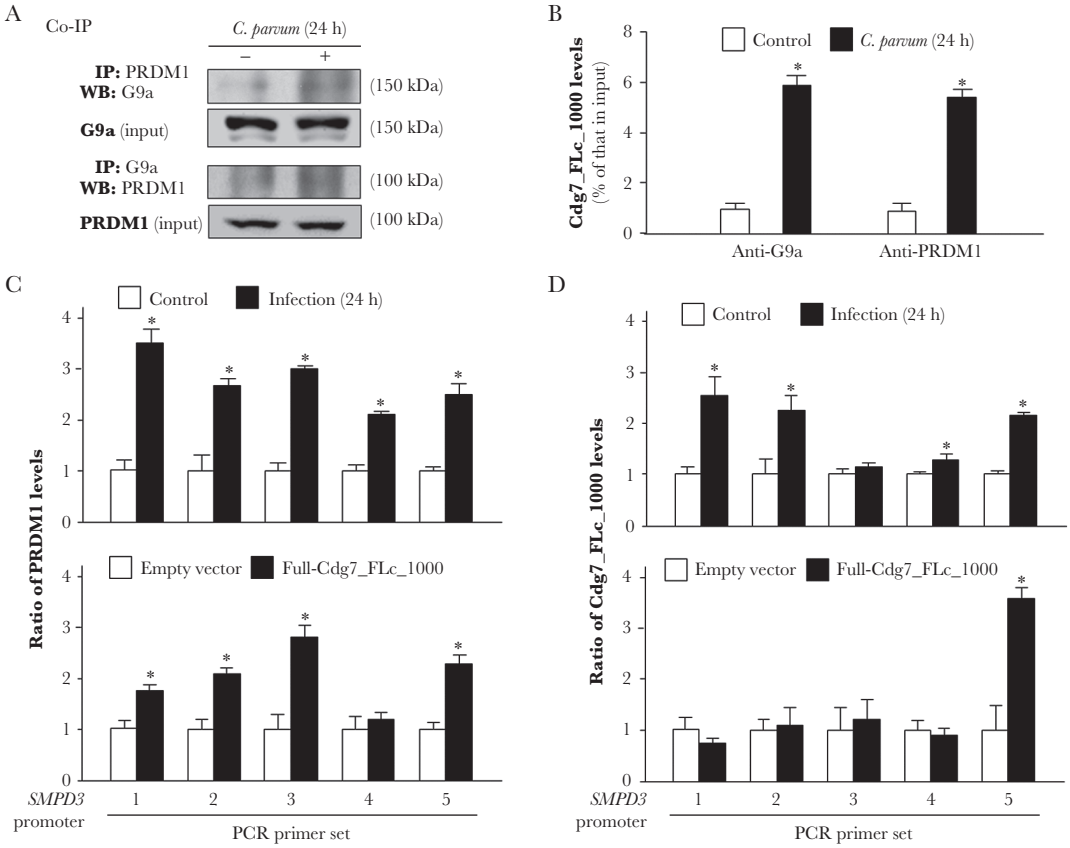

Figure 5. PRDM1 is involved in the recruitment of G9a and Cdg7_FLc_1000 to the *SMPD3* locus in cells following *Cryptosporidium parvum* infection. *A,* Increased physical association between G9a and PRDM1 in HCT-8 cells following *C. parvum* infection. Cells were exposed to *C. parvum* infection for 24 hours, followed by coimmunoprecipitation analysis (Co-IP) using anti-G9a and anti-PRDM1. *B,* Assembly of Cdg7_FLc_1000 to the G9a/PRDM1 complex in cells following *C. parvum* infection. HCT-8 cells were exposed to *C. parvum* infection for 24 hours, followed by RNA immunoprecipitation analysis using anti-G9a and anti-PRDM1. *C,* Recruitment of PRDM1 to the *SMPD3* locus in HCT-8 cells following *C. parvum* infection or transfection with Full-Cdg7_FLc_1000. Cells were exposed to *C. parvum* infection for 24 hours or transfected with Full-Cdg7_FLc_1000 for 24 hours, followed by chromatin immunoprecipitation analysis using anti-PRDM1 and the polymerase chain reaction (PCR) primer sets as designed. Increased recruitment of PRDM1 was detected in the *SMPD3* locus in cells following infection or Full-Cdg7_FLc_1000 transfection. *D,* Recruitment of Cdg7_FLc_1000 to the *SMPD3* locus in HCT-8 cells following *C. parvum* infection or transfection with Full-Cdg7_FLc_1000. Cells were exposed to *C. parvum* infection for 24 hours or transfected with Full-Cdg7_FLc_1000 for 24 hours, followed by RNA immunoprecipitation, using a pool of probes specific to Cdg7_FLc_1000 and the PCR primer sets as designed. Increased recruitment of Cdg7_FLc_1000 was detected in the *SMPD3* locus in cells following infection or Full-Cdg7_FLc_1000 transfection. Data represent means ± SEs from 3 independent experiments. **P*<.01, analysis of variance, compared with noninfected or empty vector controls.

Several pieces of evidence imply that nuclear delivery of the parasite Cdg7_FLc_1000 RNA transcript into infected cells modulates transcription of many host genes, such as *SMPD3*, contributing to alterations in the gene expression profile in host cells. First, genome-wide analysis of the gene expression profile revealed significant alterations of gene expression in cultured human intestinal epithelial cells overexpressing the Cdg7_FLc_1000 RNA. Intriguingly, many of these upregulated and downregulated genes in cells transfected with full-length Cdg7_FLc_1000 were also observed in cells following infection, including downregulation of *SMPD3*. Second, using a specific siRNA to knock down Cdg7_FLc_1000 in host cells during *C. parvum* infection attenuated the dysregulated expression of selected genes in infected cells, such as *SMPD3*. Finally, delivery of the Cdg7_FLc_1000 transcript into infected intestinal epithelial cells promoted the histone methyltransferase G9a/PRDM1–mediated H3K9 methylation associated with a specific sequence within the promoter region of the *SMPD3* locus. Moreover, the association between Cdg7_FLc_1000 delivery and trans-suppression of *SMPD3* appears to be specific, as transfection of another nuclear delivery parasite Cdg7_FLc_0990 RNA [23] failed to downregulate the expression level of *SMPD3*.

Mechanistically, downregulation of *SMPD3* in intestinal epithelial cells after *C. parvum* infection is associated with a marked increase of H3K9me3 in its gene locus. *C. parvum*–induced H3K9 methylation within the *SMPD3* locus depends on G9a, a key methyltransferase for H3K9, and is associated with the nuclear delivery of Cdg7_FLc_1000 RNA. PRDM1, a G9a-interacting protein that has been implicated in G9a-mediated histone methylation [35, 37], appears to be required for the assembly of Cdg7_FLc_1000 RNA into the G9a complex in infected cells. Therefore, *C. parvum* may hijack the G9a/PRDM1-mediated regulatory machinery through nuclear delivery of Cdg7_FLc_1000, resulting in trans-suppression of

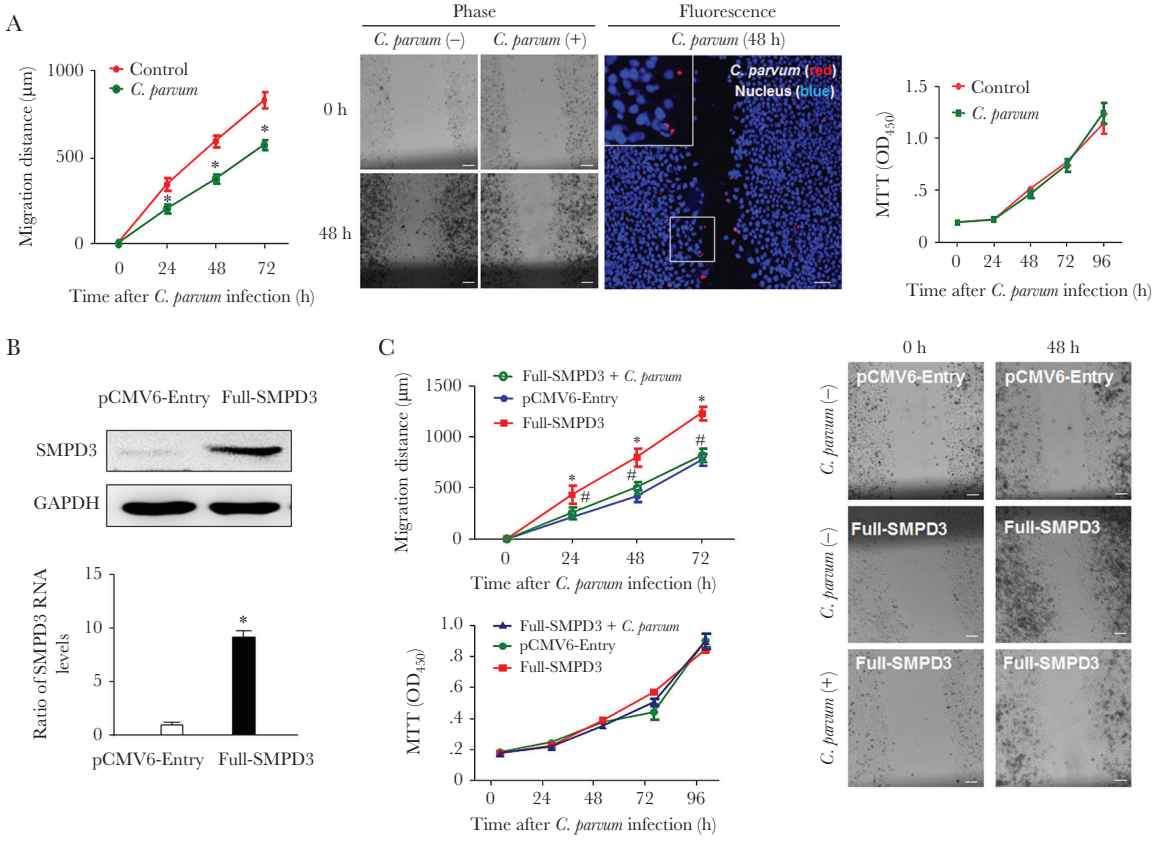

Figure 6. Inhibition of epithelial cell migration following *Cryptosporidium parvum* infection and its association with downregulation of SMPD3. *A,* Decreased migration of HCT-8 cells following *C. parvum* infection. Cell migration was assessed by measurement of the distance of cell migration after the wound-healing assay. Representative phase and dual fluorescent images of cell cultures after exposure to *C. parvum* infection for 48 hours are shown. Dual fluorescent images revealed that not only infected cells (parasite stained in red) but also noninfected cells were present at the migrating edge. Proliferation of HCT-8 cells following *C. parvum* infection was assessed by using the MTT (3-[4,5-dimethylthiazol-2-yl]-2,5-diphenyltetrazolium bromide) assay. *B,* Generation of HCT-8 cells stably expressing SMPD3. HCT-8 cells were transfected with the pCMV6-Entry-SMPD3 (Full-SMPD3) construct, and stably transfected cells were selected and confirmed by real-time polymerase chain reaction analysis and Western blot. *C,* Overexpression of SMPD3 attenuated the inhibition of cell migration induced by *C. parvum* infection. Migration of HCT-8 cells expressing the empty vector (pCMV6-Entry) and stably expressing SMPD3 was measured with or without *C. parvum* infection. Whereas a higher migration distance was detected in cells stably expressing SMPD3, a similar migration distance was observed for cells stably expressing SMPD3 following infection as compared to the noninfected control cells. No difference in cell proliferation was detected among all the treated groups. Representative phase images show the migration of stably transfected cells with or without *C. parvum* infection for 48 hours. Data represent means ± SEs from 3 independent experiments. $^{*,\#}P<.01$, by analysis of variance, compared with noninfected or empty vector controls.

SMPD3 in host cells. As an important transcriptional repressor in cell differentiation, PRDM1 acts as a master regulator of intestinal epithelium maturation [37] and is strongly expressed throughout the epithelium of the embryonic gut [42]. It orchestrates orderly and extensive reprogramming of the postnatal intestinal epithelium but is absent in the intestinal epithelial cells of adult mice [42]. Interestingly, neonatal mice are susceptible to *C. parvum* infection [26, 27], whereas adult mice are resistant to *C. parvum* infection [43]. The pathogenic role of PRDM1 in *C. parvum* infection of neonatal mice merits further exploration using conditional PRDM1 knockout mice.

Long ncRNAs in humans have been demonstrated to function as scaffold molecules to affect gene transcription through their interactions with various RNA-binding components in the chromatin-remodeling complexes [12, 44]. PRDM1 is an RNA-binding protein, with several zinc-finger C2H2 domains that can interact with DNA and RNA molecules [36, 37]. It is possible that Cdg7_FLc_1000 is assembled into the G9a complex through its interaction with PRDM1. In addition, long ncRNAs may interact with DNA molecules to form a triple-helical structure [12]. Therefore, Cdg7_FLc_1000 may guide the initial recruitment of the G9a/PRDM1 complex to the *SMPD3* locus, presumably through direct binding to a specific DNA motif in their promoter regions. Notably, transfection of host cells with a plasmid expressing Cdg7_FLc_1000 induced the recruitment of the G9a/PRDM1 complex to the *SMPD3* locus, resulting in trans-suppression of the gene in transfected cells.

How trans-suppression of *SMPD3* attenuates epithelial cell migration is still unclear; particularly, it appears that both infected and noninfected cell populations in the infected cultures show a decrease in cell migration. SMPD3 catalyzes the hydrolysis of sphingomyelin to form ceramide and phosphocholine [45]. Ceramide mediates numerous cellular

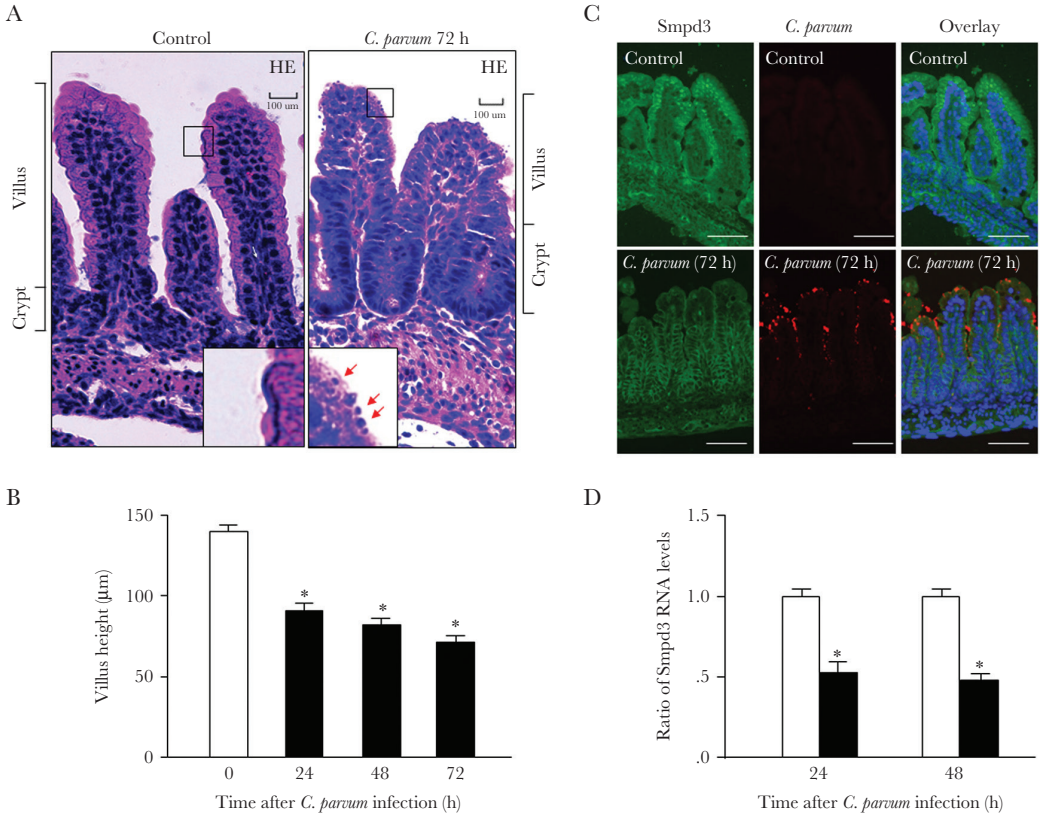

Figure 7. Downregulation of Smpd3 and shortening of the villus height of the intestinal epithelium in neonatal mice following *Cryptosporidium parvum* infection in vivo. *A,* Hematoxylin-eosin (HE) staining of ileal tissues from neonatal mice with and those without *C. parvum* infection in vivo. Neonatal mice aged 6 days received *C. parvum* oocysts by oral gavage, and ileal tissues were obtained 72 hours after parasite administration. Inserts show the selected areas at higher magnifications. Parasites attached to the lumen are indicated by arrows. *B,* Shortening of the villus height of the ileal epithelium in neonatal mice following infection. Ileal tissues were collected from 3 noninfected neonatal mice or 3 animals following *C. parvum* infection for 24, 48, and 72 hours. Tissues were processed for HE staining, and the height of the villus in the ileum was quantified. Measurements from at least 50 fields for each animal were obtained for the analysis. The bar denotes 200 μm. *C,* Decreased expression of Smpd3 in the ileal tissues of neonatal mice following *C. parvum* infection in vivo. Decreased staining was observed in the infected villi (parasites were stained in red, and Smpd3 was stained in green), compared with the noninfected crypt regions and the intestinal tissues from the noninfected animals. Nuclei of cells were stained in blue with DAPI (4′,6-diamidino-2-phenylindole). *D,* Decreased expression levels of *Smpd3* RNA were detected in the ileal tissues of neonatal mice following *C. parvum* infection. Ileal tissues were collected from noninfected neonatal mice or animals following *C. parvum* infection for 24 and 48 hours. RNA was isolated, followed by real-time polymerase chain reaction analysis of Smpd3. Data represent means ± SEs from 3 independent experiments. **P*<.01, by analysis of variance, compared with noninfected control.

functions, such as apoptosis, cell growth arrest, differentiation, cell senescence, cell migration, and adhesion [23, 24, 45–47]. Pathologically, trans-suppression of *SMPD3* in host cells through nuclear delivery of the parasite Cdg7_FLc_1000 RNA and consequent inhibition of epithelial cell migration may benefit intracellular development of the parasite after cellular internalization. The intestinal mucosa is a monolayer of rapidly self-renewing epithelial cells. New functional epithelial cells are produced from stem cells in the crypt base, differentiate, and migrate from the crypt base to the luminal surface; hence, the entire intestinal epithelium is replaced every 2–3 days in mice (and every 3–5 days in humans) [7, 48]. The complete life cycle of *C. parvum* infection requires 4–6 days [43]. Thus, inhibition of epithelial cell migration would reduce the intestinal turnover, providing an obvious benefit to the parasite's replication, as the parasite develops its intracellular stage after cellular internalization.

Supplementary Data

Supplementary materials are available at *The Journal of Infectious Diseases* online. Consisting of data provided by the authors to benefit the reader, the posted materials are not copyedited and are the sole responsibility of the authors, so questions or comments should be addressed to the corresponding author.

Notes

Acknowledgments. We thank Drs Quanghui Zhao, Yan Li, and Shibin Ma (Creighton University), for helpful and stimulating discussions; and Barbara L. Bittner (Creighton University), for her assistance in writing the manuscript.

Disclaimer. The content is solely the responsibility of the authors and does not necessarily represent the official views of the National Institutes of Health, the State of Nebraska, the Nebraska Department of Health and Human Services, or the National Natural Science Foundation of China.

Financial support. This work was supported by the National Institutes of Health (grant AI116323 to X. M. C.), the Nebraska Stem Cell Research Program (grant LB606 to X. M. C.), and the Nebraska Department of Health and Human Services (LB595 Cancer and Smoking Disease Research Program Development Grant to X. M. C.), the National Center for Research Resources (grant G20RR024001), the China Scholarship Council (to Z. M.), and the National Natural Science Foundation of China (grant 31372194 to Z. M.).

Potential conflicts of interest. All authors: No reported conflicts of interest. All authors have submitted the ICMJE Form for Disclosure of Potential Conflicts of Interest. Conflicts that the editors consider relevant to the content of the manuscript have been disclosed.

References

1. Striepen B. Parasitic infections: Time to tackle cryptosporidiosis. Nature **2013**; 503:189–91.
2. Checkley W, White AC, Jaganath D, et al. A review of the global burden, novel diagnostics, therapeutics, and vaccine targets for *cryptosporidium*. Lancet Infect Dis **2015**;15: 85–94.
3. Manabe YC, Clark DP, Moore RD, et al. Cryptosporidiosis in patients with AIDS: correlates of disease and survival. Clin Infect Dis **1998**; 27:536–42.
4. Chen XM, Keithly JS, Paya CV, LaRusso NF. Cryptosporidiosis. N Engl J Med **2002**; 346:1723–31.
5. Kotloff KL, Nataro JP, Blackwelder WC, et al. Burden and aetiology of diarrhoeal disease in infants and young children in developing countries (the Global Enteric Multicenter Study, GEMS): a prospective, case-control study. Lancet **2013**; 382:209–22.
6. Putignani L, Menichella D. Global distribution, public health and clinical impact of the protozoan pathogen *cryptosporidium*. Interdiscip Perspect Infect Dis **2010** Jul 14. pii: 753512. doi: 10.1155/2010/753512.
7. Barker N. Adult intestinal stem cells: critical drivers of epithelial homeostasis and regeneration. Nat Rev Mol Cell Biol **2014**; 15:19–33.
8. Sasahara T, Maruyama H, Aoki M, et al. Apoptosis of intestinal crypt epithelium after *Cryptosporidium parvum* infection. J Infect Chemother **2003**; 9: 278–81.
9. Savidge TC, Shmakov AN, Walker-Smith JA, Phillips AD. Epithelial cell proliferation in childhood enteropathies. Gut **1996**;39: 185–93.
10. Prasanth KV, Spector DL. Eukaryotic regulatory RNAs: an answer to the 'genome complexity' conundrum. Genes Dev **2007**; 21:11–42.
11. Bartel DP. MicroRNAs: genomics, biogenesis, mechanism, and function. Cell **2004**; 116:281–97.
12. Ulitsky I, Bartel DP. lincRNAs: genomics, evolution, and mechanisms. Cell **2013**; 154:26–46.
13. Mercer TR, Dinger ME, Mattick JS. Long non-coding RNAs: insights into functions. Nat Rev Genet **2009**; 10:155–9.
14. Chu C, Qu K, Zhong FL, Artandi SE, Chang HY. Genomic maps of long noncoding RNA occupancy reveal principles of RNA-chromatin interactions. Mol Cell **2011**; 44:667–78.
15. Donaghey J, Carey BW, Garber M, et al. lincRNAs act in the circuitry controlling pluripotency and differentiation. Nature **2011**; 477:295–300.
16. Gardner MJ, Hall N, Fung E, et al. Genome sequence of the human malaria parasite *Plasmodium falciparum*. Nature **2002**; 419:498–511.
17. Abrahamsen MS, Templeton TJ, Enomoto S, et al. Complete genome sequence of the apicomplexan, *Cryptosporidium parvum*. Science **2004**; 304:441–45.
18. Liao Q, Shen J, Liu J, et al. Genome-wide identification and functional annotation of *Plasmodium falciparum* long noncoding RNAs from RNA-seq data. Parasitol Res **2014**; 113:1269–81.
19. Vembar SS, Scherf A, Siegel TN. Noncoding RNAs as emerging regulators of *Plasmodium falciparum* virulence gene expression. Curr Opin Microbiol **2014**; 20:153–61.
20. Puiu D, Enomoto S, Buck GA, Abrahamsen MS, Kissinger JC. CryptoDB: the *Cryptosporidium* genome resource. Nucleic Acids Res **2004**; 32:D329–31.
21. Yamagishi J, Wakaguri H, Sugano S, et al. Construction and analysis of full-length cDNA library of *Cryptosporidium parvum*. Parasitol Int **2011**; 60:199–202.
22. Wang Y, Gong AY, Ma S, et al. Delivery of parasite RNA transcripts into infected epithelial cells during *Cryptosporidium* infection and its potential impact on host gene transcription. J Infect Dis **2017**; 215:636–43.
23. Hannun YA, Obeid LM. Principles of bioactive lipid signalling: lessons from sphingolipids. Nat Rev Mol Cell Biol **2008**; 9:139–50.
24. Nikolova-Karakashian M, Karakashian A, Rutkute K. Role of neutral sphingomyelinases in aging and inflammation. Subcell Biochem **2008**; 49:469–86.
25. Zhou R, Gong AY, Eischeid AN, Chen XM. miR-27b targets KSRP to coordinate TLR4-mediated epithelial defense against *Cryptosporidium parvum* infection. PLoS Pathog **2012**; 8:e1002702.
26. Kapel N, Benhamou Y, Buraud M, Magne D, Opolon P, Gobert JG. Kinetics of mucosal ileal gamma-interferon response during cryptosporidiosis in immunocompetent neonatal mice. Parasitol Res **1996**; 82:664–7.
27. Lacroix S, Mancassola R, Naciri M, Laurent F. *Cryptosporidium parvum* specific mucosal immune response in C57BL/6 neonatal and gamma interferon-deficient mice: role of tumor necrosis factor alpha in protection. Infect Immun **2001**; 69:1635–42.
28. Zhou R, Hu G, Liu J, Gong AY, Drescher KM, Chen XM. NF-kappaB p65-dependent transactivation of miRNA genes

following *Cryptosporidium parvum* infection stimulates epithelial cell immune responses. PLoS Pathog **2009**; 5:e1000681.
29. Abmayr SM, Yao T, Parmely T, Workman JL. Preparation of nuclear and cytoplasmic extracts from mammalian cells. Curr Protoc Pharmacol **2006**. doi: 10.1002/0471141755.ph1203s35.
30. Niranjanakumari S, Lasda E, Brazas R, Garcia-Blanco MA. Reversible cross-linking combined with immunoprecipitation to study RNA-protein interactions in vivo. Methods **2002**; 26:182–90.
31. Deng M, Lancto CA, Abrahamsen MS. *Cryptosporidium parvum* regulation of human epithelial cell gene expression. Int J Parasitol **2004**; 34:73–82.
32. Yang YL, Serrano MG, Sheoran AS, Manque PA, Buck GA, Widmer G. Over-expression and localization of a host protein on the membrane of *Cryptosporidium parvum* infected epithelial cells. Mol Biochem Parasitol **2009**; 168:95–101.
33. Vinayak S, Pawlowic MC, Sateriale A, et al. Genetic modification of the diarrhoeal pathogen *Cryptosporidium parvum*. Nature **2015**; 523:477–80.
34. Dong X, Weng Z. The correlation between histone modifications and gene expression. Epigenomics **2013**; 5:113–6.
35. Shinkai Y, Tachibana M. H3K9 methyltransferase G9a and the related molecule GLP. Genes Dev **2011**; 25:781–8.
36. Gyory I, Wu J, Fejér G, Seto E, Wright KL. PRDI-BF1 recruits the histone H3 methyltransferase G9a in transcriptional silencing. Nat Immunol **2004**; 5:299–308.
37. John SA, Garrett-Sinha LA. Blimp1: a conserved transcriptional repressor critical for differentiation of many tissues. Exp Cell Res **2009**; 315:1077–84.
38. Liu J, Deng M, Lancto CA, Abrahamsen MS, Rutherford MS, Enomoto S. Biphasic modulation of apoptotic pathways in *Cryptosporidium parvum*-infected human intestinal epithelial cells. Infect Immun **2009**; 77:837–49.
39. Chen XM, Levine SA, Splinter PL, et al. *Cryptosporidium parvum* activates nuclear factor kappaB in biliary epithelia preventing epithelial cell apoptosis. Gastroenterology **2001**; 120:1774–83.
40. Sibley LD. Intracellular parasite invasion strategies. Science **2004**; 304:248–53.
41. O'Connor RM, Wanyiri JW, Wojczyk BS, Kim K, Ward H. Stable expression of *Cryptosporidium parvum* glycoprotein gp40/15 in *Toxoplasma gondii*. Mol Biochem Parasitol **2007**; 152:149–58.
42. Harper J, Mould A, Andrews RM, Bikoff EK, Robertson EJ. The transcriptional repressor Blimp1/Prdm1 regulates postnatal reprogramming of intestinal enterocytes. Proc Natl Acad Sci U S A **2011**; 108:10585–90.
43. O'Donoghue PJ. *Cryptosporidium* and cryptosporidiosis in man and animals. Int J Parasitol **1995**; 25:139–95.
44. Guttman M, Donaghey J, Carey BW, et al. LincRNAs act in the circuitry controlling pluripotency and differentiation. Nature **2011**; 477:295–300.
45. Shamseddine AA, Airola MV, Hannun YA. Roles and regulation of neutral sphingomyelinase-2 in cellular and pathological processes. Adv Biol Regul **2015**; 57:24–41.
46. Stoffel W, Jenke B, Blöck B, Zumbansen M, Koebke J. Neutral sphingomyelinase 2 (smpd3) in the control of postnatal growth and development. Proc Natl Acad Sci U S A **2005**; 102:4554–9.
47. Revill K, Wang T, Lachenmayer A, et al. Genome-wide methylation analysis and epigenetic unmasking identify tumor suppressor genes in hepatocellular carcinoma. Gastroenterology **2013**; 145:1424–35.
48. Creamber B, Shorter RG, Bamforth J. The turnover and shedding of epithelial cells. I. The turnover in the gastro-intestinal tract. Gut **1961**; 2:110–8.